Resonance Raman scattering by optical phonons in unstrained germanium quantum dots

A. B. Talochkin,* S. A. Teys, and S. P. Suprun
Institute of Semiconductor Physics, Siberian Branch of RAS, 630090 Novosibirsk, Lavrentyeva 13, Russia
(Received 11 April 2005; revised manuscript received 13 July 2005; published 13 September 2005)

The position and shape of the E_1, $E_1+\Delta_1$ Raman resonance depending on the size of unstrained Ge quantum dots were studied. The dots were grown in GaAs/ZnSe/Ge/ZnSe structures on (111)-oriented GaAs substrates using molecular-beam epitaxy. A shift of the E_1 and $E_1+\Delta_1$ resonance energies by up to 0.3 eV was observed. The dependence of the shift on quantum dot size was shown to be well described by a cylindrical model using quantization of the bulk Ge electron-hole states that form excitons at the two-dimensional critical point of the interband density of states. A separate display of the E_1 and $E_1+\Delta_1$ resonances in the quantum dots related to transformation of the interband density of states into the δ function due to quantization of the energy spectrum was observed.

DOI: 10.1103/PhysRevB.72.115416 PACS number(s): 73.21.La

I. INTRODUCTION

During the past decade, numerous studies have been concerned with semiconductor quantum dot (QD) electron levels (see Refs. 1–3 for example). Attention was focused on electron-hole states of the extrema near the valence- and conduction-band edges. The effect of confinement on state energies has been well described using the envelope wave-function method in the effective-mass approximation.[4] Yet, few attempts have been made to study the electron states that form the critical points in the interband density of states with energies far from the fundamental band gap. A good example is the two-dimensional critical point of Ge responsible for the E_1, $E_1+\Delta_1$ Raman resonance observed in bulk Ge (Ref. 5) and Ge QDs. This resonance has been recently studied in Ge QDs obtained by different methods.[6–11] The E_1, $E_1+\Delta_1$ resonance energy in QDs was shifted by up to 0.7 eV as compared to its bulk position. The observed shift value was shown to be well described by quantization of the ground-state energy of a two-dimensional exciton or a particle in a "quantum box."[8,7] However, the QD systems used in the experiments had undesirable features that did not allow a detailed study of the nature of the observed resonance.[6–11] The QDs formed by implantation of Ge^+ ions into SiO_2 with a subsequent annealing have a sufficiently large QD size distribution leading to an additional broadening of the resonance.[6,8] The Ge QDs obtained in a Si matrix using the self-organized growth in the process of molecular-beam epitaxy (MBE) are strongly strained.[7,9,10] The mechanical stresses that produce a distortion of electron spectrum are considerably nonuniform in such Ge QDs (Refs. 3 and 11). This complicates the analysis of the behavior and nature of the observed resonance. In this work, we studied the E_1, $E_1+\Delta_1$ Raman resonance in the unstrained Ge QDs grown in GaAs/ZnSe/Ge/ZnSe structures using MBE. In this system, the array of QDs has a sufficiently narrow width of the size distribution function (10%), the absence of mechanical stress is determined by the similarity of the lattice constants of materials (the mismatch is less than 0.3%). This allowed us to investigate the position and amplitude of the E_1, $E_1+\Delta_1$ Raman resonance in Ge QDs of different sizes, to observe unique features that clarify its nature, and to apply the spectrum of the electron states of bulk Ge for analysis of experimental results.

II. EXPERIMENTAL

The GaAs/ZnSe/Ge/ZnSe structures with Ge QDs were grown in an MBE system with a residual gas pressure of 10^{-8} Pa. The growth chamber was equipped with a high-energy electron diffractometer for analysis of the surface structure. Thermal evaporators were used as sources of germanium and zinc selenide. ZnSe was grown from the compound. GaAs (111) wafers were used as substrates. The substrates underwent a standard chemical treatment. Then, they were fixed on a molybdenum carrier with an indium-gallium eutectic and placed into the chamber. An atomically clean surface was obtained in the process of thermal cleaning of the GaAs substrates at $T=580$ °C, which fact was confirmed by the appearance of diffraction images corresponding to the surface superstructures. An epitaxial ZnSe layer 500-Å thick was grown at $T=230$ °C. The obtained surface had a (2×1) superstructure stabilized by selenium. Then, a Ge layer with an effective thickness in the range of 5–60 Å was deposited at $T\approx100$ °C. Next, Ge was covered with a thin ZnSe layer (20–40 Å) at the same temperature. A protective ZnSe layer 500-Å thick was grown last at $T=230$ °C.

The lattice constants of GaAs, ZnSe, and Ge are identical within 0.3% (Ref. 12), making the mechanical strain in the grown structures negligibly small. In such a case, the mechanism of Ge QDs growth significantly differs from the Sranski-Krastanov mechanism that works in strained systems (Ge-Si).[13] Amorphous Ge grows at a deposition rate of 1 Å/min and at a substrate temperature $T<90$ °C, while a two-dimensional crystalline film forms at $T>130$ °C. The island mechanism of growth appears at temperatures in the range of 90–130 °C. The sizes of the Ge islands formed at the early growth stage increase with increasing the effective deposited thickness until the islands finally merge into a continuous layer. Varying the thickness of the Ge layer, we could obtain structures with QDs of different sizes whose dimensions in the growth plane varied in the range of 50–300 Å.

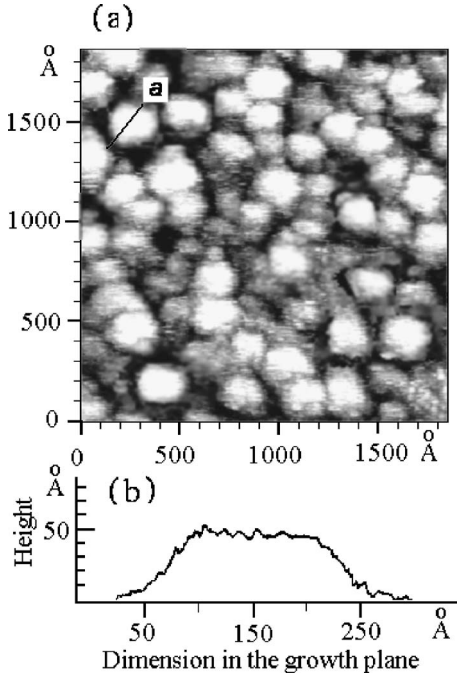

FIG. 1. (a) STM image of an 1800×1800 Å surface of a sample with Ge QDs, and (b) the profile measured along the line labeled *a*.

The size and shape of Ge islands were measured with a Riber-Omicron scanning tunneling microscope (STM) on samples not covered with the last ZnSe layers. Figure 1(a) presents an STM image of the 1800×1800 Å surface area of a sample with an effective Ge thickness of 34 Å obtained at a tunneling current of 0.2 nA. A profile measured along the line *a* is shown in Fig. 1(b). The Ge islands had the appearance of drops with flat tops. As seen in Fig. 1(b), the characteristic size of the Ge islands is 200 Å in the growth plane and the height is 50 Å. A statistical analysis of images that included as many as 10^3 Ge islands demonstrated that the half-width of the size distribution function did not exceed 10% for the most uniform QD arrays.

The spectra of Raman scattering by optical phonons for the obtained GaAs/ZnSe/Ge/ZnSe structures were measured at room temperature in a near-backscattering geometry. The spectra were excited by the discrete lines of an Ar^+ laser and were recorded with a double diffraction grating spectrometer. Resonance curves were measured using a dye laser (Spectra Physics, model 375) pumped by a 10-W Ar^+ laser. Three laser dyes, Rhodamine 6G, 110, and Coumarin 510, were used to obtain excitation light with an energy tuned in the range of 2.0–2.4 eV. The spectral range of 2.4–2.7 eV was covered with discrete lines of the Ar^+ laser. The observed intensities of the phonon peaks were corrected by taking into account the spectral dependence of the bulk Ge absorption coefficient, the factor of ω,[4] and the sensitivity of the measuring system. The latter was determined using the intensity of the Raman peaks in calcite.

III. RAMAN E_1, $E_1+\Delta_1$ RESONANCE IN Ge QUANTUM DOTS

We studied the spectra of Raman scattering by optical phonons in the CaAs/ZnSe/Ge/ZnSe structures with Ge QDs. The analyzed samples were stepped with the effective thickness of the Ge layer *d* varying in the 5–60 Å range. The nucleation of Ge islands and a subsequent increase in their sizes up to their merger into a continuous Ge layer took place in this layer thickness range at the above growth conditions. A CaAs/ZnSe/Ge/ZnSe structure obtained on the (111) surface is shown schematically in the inset of Fig. 2. The regions ***a*-*c*** contain arrays of isolated Ge islands. The effective thickness of Ge layer is 6, 15, and 34 Å, respectively. Region ***d*** ($d=56$ Å) contains a continuous Ge layer. According to the STM data, a characteristic island height is $h\approx20$ Å and base size in the growth plane is $D\approx60$ Å for the effective thickness of Ge layer $d=6$ Å. For $d=15$ and 34 Å, these parameters are $h\approx37$ Å, $D\approx120$ Å and $h\approx50$ Å, $D\approx200$ Å, respectively. Figures 2(b)–2(d) show the Raman spectra obtained from the ***b*–*d*** regions of the CaAs/ZnSe/Ge/ZnSe structure at room temperature using the excitation light wavelength $\lambda=488$ nm. The optical-phonon lines of the ZnSe matrix (LO -255 cm^{-1}), the GaAs substrate (TO -273 cm^{-1}, LO -294 cm^{-1}), and the Ge layer (TO+LO -300 cm^{-1}) are clearly seen in the given spectra. The position of the Ge peak and the ratio of its intensities obtained in different polarization geometries agree well with their bulk values. This means that there is neither mechanical stress in the QDs nor measurable deviation of Ge orientation from the crystallographic directions determined by the substrate. The Ge QD phonon peak intensity is unusually high, being by five times greater than the bulk intensity measured with the same excitation wavelength [Figs. 2(b) and 2(c)]; it changes abruptly as soon as Ge QDs merge into a continuous layer [Fig. 2(d)]. Such a behavior is caused by change in the E_1, $E_1+\Delta_1$ resonance energy in Ge QDs as compared with

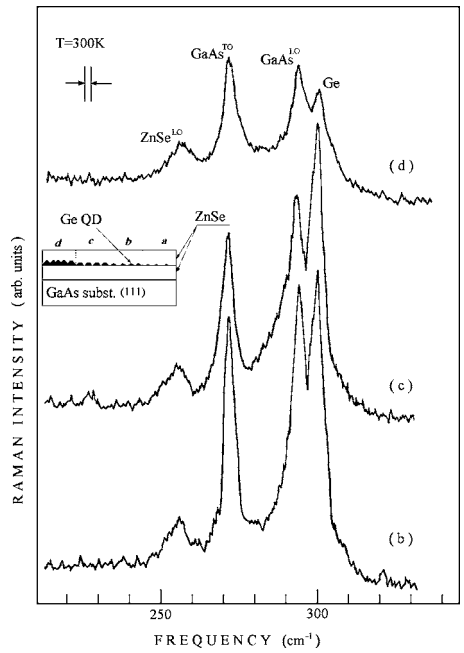

FIG. 2. Raman spectra of the GaAs/ZnSe/Ge/ZnSe structure shown in the inset. The spectra (b) and (c) were obtained from the regions with QDs (the effective thicknesses *d* of the Ge layer are 15 and 34 Å, respectively). The spectrum (d) was taken from the region with a continuous Ge layer ($d=56$ Å).

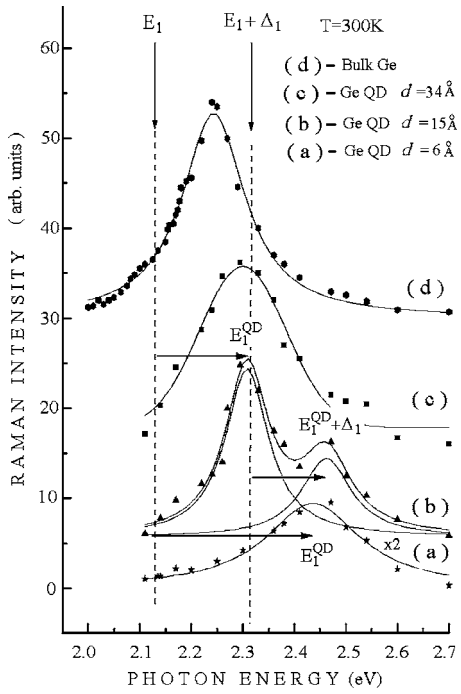

FIG. 3. Resonance curves of Raman scattering by optical phonons in Ge QDs [(a)–(c)] and in bulk Ge (d). The experimental points are denoted by symbols. The best-fit approximation of the experimental dependencies by Lorenz contours are given by the solid lines. The energy shifts of the E_1 and $E_1+\Delta_1$ resonances are shown by the horizontal arrows.

that of bulk material. The considerable difference between the optical-phonon frequencies of Ge and ZnSe (45 cm^{-1}) means that Ge optical phonons are strongly localized in QDs. This enabled us to study electron states of Ge QDs using resonant Raman scattering by optical phonons.

We note that, as it is seen in Fig. 2, the phonon line intensities of the GaAs substrate decrease with increasing the thickness of the Ge layer due to absorption of excitation and scattered light in this layer. This allows the absorption coefficient $\boldsymbol{\alpha}_1$ of the Ge layer with QDs to be obtained. Since ZnSe is transparent in the considered energy range, the observed Raman intensity can be written as $I=I_0\exp(-2\alpha_1 d)$, where I_0 is the intensity measured on a structure without a Ge layer. Our measurements have shown that the value of α_1 does not differ from the bulk value within an accuracy of ±10%. Despite a considerable modification of the interband density of states and the shift of the E_1, $E_1+\Delta_1$ resonance energy in QDs, which will be considered below, the value of the absorption coefficient change is insignificant. This feature may be explained by the fact that the main contributions to absorption are give by optical transitions that are not related to the E_1, $E_1+\Delta_1$ resonance.

The resonance dependencies of Raman scattering by optical phonons of bulk Ge and Ge QDs were analyzed to get detailed information on the E_1, $E_1+\Delta_1$ resonance behavior with the QD sizes. Figure 3 shows the resonance curves measured at room temperature in the energy range of 2.0–2.7 eV. The experimental points are denoted by symbols. The solid lines indicate the best-fit approximation of the experimental data by Lorenz contours done to obtain the accurate values of the resonance positions and half-widths. The curve (d) was observed in bulk Ge with the (111) surface This curve agrees fairly well with the data previously reported by Cerdeira *et al.*[5] The vertical arrows in Fig. 3 indicate the positions of the E_1 and $E_1+\Delta_1$ transitions in Ge. The resonance curves (a)–(c) were measured in the regions of the CaAs/ZnSe/Ge/ZnSe(111) structure with Ge QDs shown in the inset of Fig. 2. The effective thickness of the Ge layer for these regions is 6, 15, and 34 Å, respectively. The resonance dependencies shown in Fig. 3 were measured using the same sensitivity of the registration system and scattering geometry. This allowed us to directly compare the resonance intensities and their positions in the QDs with those in bulk Ge. Since Raman intensity is proportional to the scattering volume, the resonance amplitudes observed in the QDs [Figs. 3(a)–3(c)] should be multiplied by the amount L/d [where $L=(2\alpha)^{-1}=100$ Å is the light penetration depth in Ge and α is the Ge absorption coefficient]. The obtained QD resonance amplitudes exceed those of the bulk by factors of 2.9, 6.6, and 4 for the (a), (b), and (c) curves, respectively (Fig. 3). As seen in Fig. 3, the resonance curve of large QDs [$D\approx 200$ Å, $h\approx 50$ Å, Fig. 3(c)] is shifted towards the high-energy side from the bulk position of the resonance by 50 meV. We attribute this shift to the change of both the E_1 and $E_1+\Delta_1$ resonance energies by this value. The resonance dependence of the smaller QDs [$D\approx 120$ Å, $h\approx 37$ Å, Fig. 3(b)] exhibits two peaks that we considered as a separate appearance of the E_1 and $E_1+\Delta_1$ resonances. The horizontal arrows in Fig. 3(b) indicate the energy shifts observed for these resonances. One peak of the E_1 resonance shifted by 0.3 eV is observed in QDs of minimum sizes [$D\approx 60$ Å, $h\approx 20$ Å, Fig. 3(a)]. The absence of the $E_1+\Delta_1$ peak in curve (a) will be discussed in Sec. V. Thus, an increase of the Raman cross section by optical phonons, a shift of the E_1 and $E_1+\Delta_1$ resonance energies, and also a separate appearance of these resonances are specific features observed in the array of unstrained Ge QDs obtained in a ZnSe matrix.

IV. QUANTIZATION OF THE QD ELECTRON-HOLE SPECTRUM

Let us consider the observed shift of E_1, $E_1+\Delta_1$ resonance energy in Ge QDs using the spectrum of electron states of bulk Ge. Figure 4(a) shows the energy bands of Ge in the (111) direction of the $\boldsymbol{k}$ space calculated in Ref. 14 by the ($\boldsymbol{k}$-$\boldsymbol{p}$) method. The (Λ_1) electron and the ($\Lambda_{4,5}$, Λ_6) hole bands are nearly parallel along the (111) direction in the major part of the Brillouin zone. This band structure creates a two-dimensional critical point of the interband density of states that results in the E_1, $E_1+\Delta_1$ Raman resonance observed in bulk Ge (Ref. 5). The positions of the conduction (E_c)- and valence (E_v)-band edges of ZnSe are marked in Fig. 4(a) with horizontal lines.[12] The electron and hole states of Ge QDs in the ZnSe band gap [between the E_c and E_v levels, Fig. 4(a)] are localized. The electron and hole energy bands in the ($\boldsymbol{k}_x$,$\boldsymbol{k}_y$) plane perpendicular to the (111) direction are shown in Fig. 4(b) for the $\boldsymbol{k}_z$ value designated in Fig. 4(a) as arrows (A). These bands are well described at $\boldsymbol{k}_{x,y}$

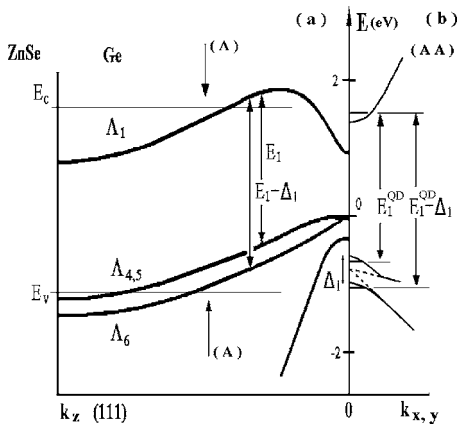

FIG. 4. (a) Energy spectrum of bulk Ge calculated in Ref. 14 for the (111) direction. The horizontal lines E_c and E_v indicate the positions of the ZnSe band edges. (b) Dispersion of the electron and hole bands in the $\boldsymbol{k}_{x,y}$ plane perpendicular to the (111) direction at the point (A) of the momentum $\boldsymbol{k}_Z$.

~ 0 by the effective-mass approximation. The effective mass $m_\perp$ of the E_1 and $E_1+\Delta_1$ transitions in this direction is $0.045m_0$ (m_0 is the free-electron mass).[15] The hole bands at $\boldsymbol{k}_{x,y} \approx 0$ that include the spin-orbit interaction are indicated by the solid lines and those that do not by the dashed lines in Fig. 4(b).

The QD size in the growth plane is comparable to the Bohr radius of interband exciton expressed as $(\hbar^2\varepsilon/m_\perp e^2) \approx 180$ Å, where $\hbar$ is the Planck constant, $\varepsilon=15.8$ is the dielectric constant of Ge, and e is the electron charge.[16] Hence, a consideration of the localized potential related to the ZnSe matrix should include the Coulomb interaction between an electron and a hole. The exciton effects have been calculated by Kane in Ref. 16 for the case of a saddle critical point [$m_\parallel \gg m_\perp$, where $m_\parallel$ is the reduced effective mass of an electron and a hole in the z-(111) direction]. It was shown that the adiabatic approximation allows one to separate the z and (x,y) variables in the Schrödinger equation for the exciton envelope wave function. As a result, this function can be chosen as a plane wave $\exp(ik_z z)$ for the (111) direction, where k_z is the exciton wave vector. The real drop-shaped form of QDs [Fig. 1(b)] can be approximated by a cylinder of height h in the (111) direction and radius r in the perpendicular plane. It is easy to see that exciton states with envelope functions in the form of standing waves with $k_z = \pi n/2h$ (n is an integer) satisfy the boundary conditions for this QD model. As a result, the continuous spectrum of excitons transforms into a set of discrete levels in QDs. The states with the minimum wave vector ($k_z=\pi/2h$) give the main contribution to the QD interband density of states due to momentum conservation. The confinement of the excitons in this direction does not change the E_1, $E_1+\Delta_1$ resonance energy because of the high reduced effective mass ($m_\parallel > 50m_\perp$), as mentioned in Ref. 8.

The confinement of excitons in the (x,y) plane leads to the quantization of their spectrum. The ground-state energies for electrons and holes are indicated by horizontal lines in Fig. 4(b). A change in these energies with the QD size results in a shift of the E_1 and $E_1+\Delta_1$ resonance positions. The

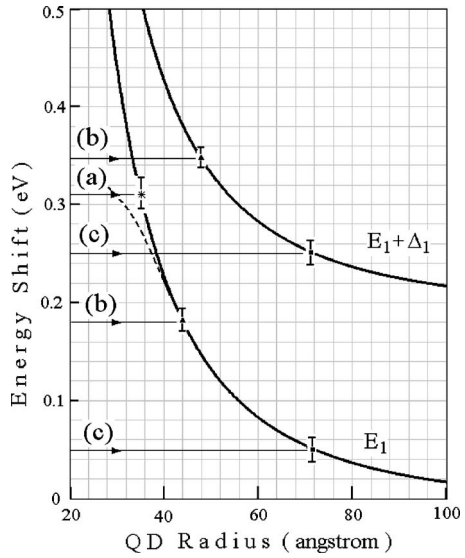

FIG. 5. Dependence of the E_1 and $E_1+\Delta_1$ resonance energy shifts on the radius of cylinder $\boldsymbol{r}$ in the growth plane. The curves shown by the solid lines were calculated using Eq. (1). The observed positions of the resonances in QDs are shown by the symbols.

energy shift ΔE of the exciton ground state obtained from the Schrödinger equation for the exciton envelope wave function has the form[8]

$$\Delta E = \frac{2}{2m_\perp}\left(\frac{2.4}{r}\right)^2 - \frac{3.51e^2}{\varepsilon \cdot r}. \quad (1)$$

The first term in Eq. (1) is the energy shift of the electron and hole ground states resulting from the confinement. The second term, resulting from the electron-hole Coulomb interaction, was obtained using the perturbation theory.[8]

The theoretical dependencies of the E_1 and $E_1+\Delta_1$ resonance energy shifts calculated from Eq. (1) as functions of the QD radius are shown in Fig. 5 by the solid lines. The resonance energy values obtained for the Ge QDs [see Figs. 3(a)–3(c)] are projected to the theoretical curves, as shown by horizontal arrows (a), (b), and (c) in Fig. 5. The same symbols in Figs. 3 and 5 refer to one and the same regions of the structure with QDs. The abscissas of the corresponding data points then determine the values of r, which were found to be 35, 45, and 72 Å for the regions ***a***, ***b***, and ***c***, respectively. For the QDs of sufficiently large sizes (***b*** and ***c***) with the resonance shifts smaller than $\Delta_1=0.2$ eV, the cylindrical model determines values of r that are by 25% smaller than the QD base radii obtained by STM measurements. This inconsistency can be attributed to sensitivity of the envelope wave function to an effective (averaged) QD lateral surface. The radius of the cylinder used to approximate the actual QD shape can be expected to be smaller than the QD radius at the QD base. From the actual QD shape [see Fig. 1(b)], it can be seen that the cylinder radius intersecting its lateral surface at about half its height is by 25% smaller than the QD base. As a result, the thus corrected QD model describes well the observed change in the E_1 and $E_1+\Delta_1$ resonance energy dependence on the QD size. As to QDs of smaller sizes [Fig.

3(c)], the radius determined from Fig. 5(c) (35 Å) was found to be somewhat greater than the real value (30 Å). This difference can be explained by the effect of finite height of the potential barrier related to the ZnSe matrix on the energy position of QD states. For small QDs, the energy shift of QD states is large ($\Delta E \geqslant \Delta_1$). As a result, a part of the electron and hole states are close to the edges of the ZnSe potential barriers [Fig. 4(a), E_c, E_v], where the dependence of ΔE on r deviates from the one obtained theoretically for the infinite barrier [Eq. (1)]. A qualitative shape of this dependence is indicated by the dashed line in Fig. 5. As it is seen, this allows us to clarify the obtained difference. The effect of the finite barrier height is the most probable cause of the observed deviations for small QDs. Thus, the simplest model of quantization of the electron-hole spectrum in bulk Ge well explains the observed shift of the E_1 and $E_1+\Delta_1$ resonance energies versus QD size.

V. INTENSITY AND SHAPE OF THE RAMAN RESONANCE IN QDS

The unique features of the Raman resonance in Ge QDs are: (1) separate appearance of the E_1 and $E_1+\Delta_1$ resonances and (2) increased amplitude of these resonances as compared with the bulk case (see Fig. 3). Let us consider these features in more detail. The frequency dependence of Raman scattering by optical phonons in the range of the E_1, $E_1+\Delta_1$ resonance for the three-band processes, which dominate in this case, is given by[5]

$$I(\omega) \sim |\chi^-(\omega) - \chi^+(\omega)|^2, \tag{2}$$

where $\chi^-(\omega)$ and $\chi^+(\omega)$ are the electronic susceptibilities of the E_1 and $E_1+\Delta_1$ transitions, respectively. Omitting the frequency independent multipliers, Eq. (2) can be rewritten in the form[17]

$$I(\omega) \sim \left| \int \left(\frac{\rho_2(\omega_1)}{\omega - \omega_1 - \imath\Gamma} - \frac{\rho_1(\omega_1)}{\omega - \omega_1 - \imath\Gamma} \right) d\omega_1 \right|^2, \tag{3}$$

where $\rho_1(\omega)$ and $\rho_2(\omega)$ are the interband densities of the states for the E_1 and $E_1+\Delta_1$ transitions, respectively, and Γ is the damping parameter of involved electron-hole states. The $\rho_1(\omega)$ and $\rho_2(\omega)$ have the form of steps of height $\rho_0 = K_z m_\perp / \hbar^2 \pi^2$ located at the energies of the E_1 and $E_1+\Delta_1$ resonances [$K_z \approx 0.3\pi/a_0$ is the extension of the critical point in the z-(111) direction and a_0 is the lattice constant] for the two-dimensional critical point with parabolic bands in the plane normal to the (111) direction. The resonant curve calculated for the steps of width 0.15 eV and $\hbar\Gamma = 50$ meV from Eq. (3) is shown in Fig. 6(a). The curve is seen to be in good qualitative agreement with the experimental dependence of Fig. 3(d). A similar agreement was obtained in Ref. 5 using the experimental dependences of the $\chi^-(\omega)$ and $\chi^+(\omega)$. Since the considered model is valid near the E_1 and $E_1+\Delta_1$ gaps (i.e., for an ideal critical point) it provides only a qualitative agreement with the experiment. Nevertheless, it allows one to understand the nature of the change in the resonance shape and intensity observed as we pass from the bulk case to a QD.

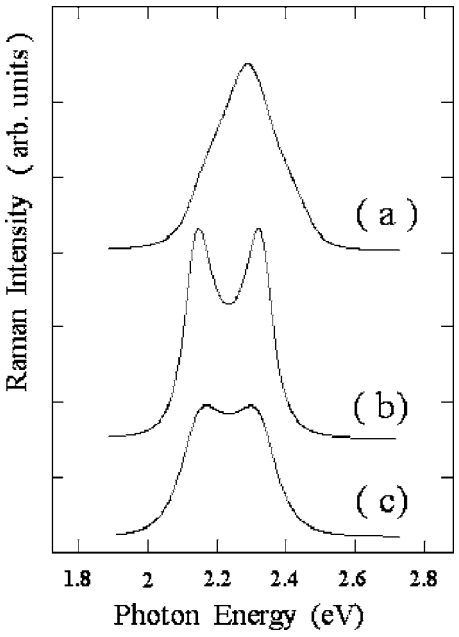

FIG. 6. (a) Resonance curves of Raman scattering by optical phonons calculated for bulk Ge using Eq. (3), for a separate QD (b), and for a QD array with the dispersion of QD sizes taken into account according to Eq. (4).

From the consideration of the electron-hole spectrum quantization it follows that the interband density of states is transformed into $4K\,\delta(\hbar\omega_1 - E^{QD})$ for a QD, where E^{QD} is the ground-state energy of the E_1 or $E_1+\Delta_1$ transition, K is the degree of degeneracy of the QD exciton states per unit of volume. Equation (3) appears for a QD in the form

$$I^{QD}(\omega) \sim \left| \frac{1}{\omega - E_1^{QD} - i\Gamma} - \frac{1}{\omega - E_1^{QD} - \Delta_1 - i\Gamma} \right|^2 K^2. \tag{4}$$

The resonance curve calculated from Eq. (4) without the inclusion of the resonance shift is shown in Fig. 6(b). Here, the peaks of the E_1 and $E_1+\Delta_1$ resonances are separate from each other because the interband density of states transforms into the δ function. The experimental dependence [Fig. 3(b)] shows that the amplitude of the $E_1+\Delta_1$ peak is two times smaller than that of the E_1 peak. This is because a part of the electron and hole states that form the considered critical point appears in the range of the continuous spectrum of the ZnSe matrix (above the E_c and below the E_v levels), as seen in Fig. 4. These states are delocalized and strongly damped. Their damping parameter Γ can considerably increase as a result of decay of these states into states of the matrix spectrum. Because the intensity of the observed resonance is proportional to $(\Gamma)^{-2}$, the contribution of these damped states to Raman scattering becomes negligibly small in comparison with that of the QD localized states. As it is seen in Fig. 4(a), the number of the localized hole states of the Λ_6 band above the E_v level determining the intensity of the $E_1+\Delta_1$ resonance is smaller than the number of states of the $\Lambda_{4,5}$ band responsible for the E_1 resonance intensity. The peak of the E_1 resonance is only observed in QDs of small size [Fig. 3(a)]. In such a case, all the states of the Λ_6 and partly of the $\Lambda_{4,5}$

bands turn out to be shifted into the range of the ZnSe matrix spectrum. As a consequence, the $E_1+\Delta_1$ resonance is not observed and the intensity of the E_1 resonance decreases. Thus, the separate appearance of the E_1 and $E_1+\Delta_1$ resonances in QDs results from the transformation of the interband density of states into the δ function, and the difference in the resonance intensities can be attributed to the effect of the matrix on the QD electron-hole states.

The real QD array has a finite value of dispersion of QD sizes and a variation of QD shapes. These factors produce a dispersion of the considered resonance energy in the QD array and determine the shape of the observed resonance curve. Assuming that the dispersion of the resonance energy is $f(E)=\exp(-|E^{QD}-E|/\beta)$ and using Eq. (4), the resulting resonance curve can be obtained. The (c) curve shown in Fig. 6 is calculated for the value $\beta=20$ meV. In this case, the peaks of the E_1 and $E_1+\Delta_1$ resonances merge into one (they can hardly be distinguished from one another), and the resonance curve is twice as wide as that of a separate resonance. This is the case observed for the array of sufficiently large QDs that are just about to merge into a continuous Ge layer [Fig. 3(c)], when inhomogeneities of the above nature increase. The half-width of this curve is 0.22 eV, whereas that of the separate resonance curves is 0.1 eV [Fig. 3(b)]. The value $\beta=20$ meV used in the calculation corresponds to the size distribution function with a half-width of 40%, which agrees with the STM data. This effect of the merger of the E_1 and $E_1+\Delta_1$ peaks due to geometrical inhomogeneities in the QD array is apparently a typical feature for all the earlier reported experiments.[6–10]

Since Eqs. (3) and (4) are related to a unit volume, the ratio of the resonance amplitudes can be estimated. The Raman intensity determined by Eq. (3) can be estimated at the resonance as $I\approx\rho_0^2[4\Delta_1^2/(\Delta_1^2+4\Gamma^2)]^2\approx(4\rho_0)^2$. Taking into account that $K=n_zN_0$, where N_0 is the number of QDs per volume and n_z is the degeneracy degree of QD exciton states along the z-(111) direction, we have

$$\frac{I^{QD}}{I}\approx\left(\frac{\pi^2 n_z N_0}{K_z\Gamma m_\perp}\right)^2. \tag{5}$$

The unknown value of n_z can be found using the experimental resonance intensity ratio $I^{QD}/I\sim 10$. The n_z value estimated in this way is $\sim 10^2$. This value determines the number of exciton states with $k_z=\pi/2h$ in the range of the given QD resonance. These states give the major contribution to the QD interband density of states due to the momentum conservation. The number of states in QDs originating from separate bulk bands [$\Lambda_{4,5}$, Λ_6 valence, and Λ_1 conduction, Fig. 4(a)] should not differ considerably from the estimated value ($\sim 10^2$). Assuming that these states are spaced equidistantly, we can estimate the energy spacing δE between them. Starting from the bulk spectrum [Fig. 4(a)] we have found $\delta E\approx 8$ meV, which is considerably smaller than the Ge optical-phonon energy (37 meV). The relaxation of photoexcited carriers should then proceed efficiently in this energy range by one-phonon emission, as in bulk Ge. In contrast, for the case of $\delta E>37$ meV, the relaxation rate should be reduced significantly because multiphonon emission is a much less probable process. An ultrafast relaxation of photoexcited carriers in Ge QDs was observed by Tognini *et al.*[18] Our estimation of the number of states in this Ge QD energy range explains the nature of this ultrafast process. Thus, the large number of states of the two-dimensional critical point of Ge QDs determines the intensity of Raman resonance and, in addition, explains the ultrafast relaxation of photoexcited carriers experimentally observed in Ref. 18.

VI. CONCLUSIONS

The position and shape of the E_1, $E_1+\Delta_1$ Raman resonance depending on the size of unstrained Ge quantum dots were studied. A shift of the E_1, $E_1+\Delta_1$ resonance energy by up to 0.3 eV was observed with decreasing the QD size. The shift was shown to be well described by a cylindrical model using quantization of the bulk Ge electron-hole states that form excitons at the two-dimensional critical point of the interband density of states. Two separate peaks of the E_1 and $E_1+\Delta_1$ resonances were observed in a sufficiently homogenous QD array. Their separate appearance is shown to be determined by transformation of the interband density of states into the δ function due to the quantization of spectrum. The observed shape of the resonance is well described by taking into account the interband density of states, the dispersion of QD sizes, and the effect of the ZnSe matrix spectrum on the QD electron-hole states. The observed increase in the QD resonance intensities in comparison with bulk Ge can be attributed to a large number of QD discrete states originating from the valence and conduction bands in the (111) direction.

ACKNOWLEDGMENTS

We would like to thank A.V. Prozorov for his help with the MBE growth of the investigated structures. This work was supported by the Russian Foundation for Basic Research (Grant No. 04-02-16425).

*Email address: tal@thermo.isp.nsc.ru

[1] T. Takagahara and K. Takeda, Phys. Rev. B **46**, 15578 (1992).
[2] Y. Maeda, Phys. Rev. B **51**, 1658 (1995).
[3] M. Grundmann, O. Stier, and D. Bimberg, Phys. Rev. B **52**, 11969 (1995).
[4] L. Banyai and S. W. Koch, in *Semiconductor Quantum Dots*, World Scientific Series on Atomic, Molecular and Optical Physics, Vol. 2 (World Scientific, Singapore, 1993).
[5] F. Cerdeira, W. Dreybrodt, and M. Cardona, Solid State Commun. **10**, 591 (1972).
[6] Y. Sasaki and C. Horie, Phys. Rev. B **47**, 3811 (1993).
[7] A. B. Talochkin, V. A. Markov, S. P. Suprun, and A. I. Nikiforov,

JETP Lett. **64**, 219 (1996).
[8] K. L. Teo, S. H. Kwok, P. Y. Yu, and Soumyendu Guha, Phys. Rev. B **62**, 1584 (2000).
[9] K. L. Teo, L. Qin, Z. X. Shen, and O. G. Schmidt, Appl. Phys. Lett. **80**, 2919 (2002).
[10] L. Qin, K. L. Teo, Z. X. Shen, C. S. Peng, and J. M. Zhou, Phys. Rev. B **64**, 075312 (2001).
[11] A. B. Talochkin, V. A. Markov, A. I. Nikiforov, and S. A. Teys, JETP Lett. **70**, 288 (1999).
[12] S. P. Kowalczyk, E. A. Kraut, J. P. Waldrop, and R. W. Grant, J. Vac. Sci. Technol. **21**, 482 (1982).
[13] Y.-W. Mo, D. E. Savage, B. S. Swartzentruber, and M. G. Legally, Phys. Rev. Lett. **65**, 1020 (1990).
[14] F. Pollak and M. Cardona, Phys. Rev. **142**, 530 (1966).
[15] D. E. Aspnes, Phys. Rev. Lett. **31**, 230 (1973).
[16] E. O. Kane, Phys. Rev. **180**, 852 (1969).
[17] K. P. Jain and Gayatri Choudhury, Phys. Rev. B **8**, 676 (1973).
[18] P. Tognini, A. Stella, S. De Silvestri, M. Nisoli, S. Stagira, P. Cheyssac, and R. Kofman, Appl. Phys. Lett. **75**, 208 (1999).